SEPARATION OF MAIN AND TAIL ROTOR NOISE SOURCES FROM GROUND-BASED ACOUSTIC MEASUREMENTS USING TIME-DOMAIN DE-DOPPLERIZATION

Eric Greenwood
NASA Langley Research Center
Hampton, Virginia, USA

Fredric H. Schmitz
University of Maryland
College Park, Maryland, USA

ABSTRACT

A new method of separating the contributions of helicopter main and tail rotor noise sources is presented, making use of ground-based acoustic measurements. The method employs time-domain de-Dopplerization to transform the acoustic pressure time-history data collected from an array of ground-based microphones to the equivalent time-history signals observed by an array of virtual inflight microphones traveling with the helicopter. The now-stationary signals observed by the virtual microphones are then periodically averaged with the main and tail rotor once per revolution triggers. The averaging process suppresses noise which is not periodic with the respective rotor, allowing for the separation of main and tail rotor pressure time-histories. The averaged measurements are then interpolated across the range of directivity angles captured by the microphone array in order to generate separate acoustic hemispheres for the main and tail rotor noise sources. The new method is successfully applied to ground-based microphone measurements of a Bell 206B3 helicopter and demonstrates the strong directivity characteristics of harmonic noise radiation from both the main and tail rotors of that helicopter.

LIST OF SYMBOLS

a_0	Speed of sound in the acoustic medium
d	Distance between real and assumed source
f_s	Sampling frequency
M	Mach number
M_o	Mach number of observer
M_r	Mach number of source with respect to medium along propagation direction
p'	Acoustic pressure at observer
q	Acoustic source strength
Q	Compact source strength
r	Straight-line propagation distance
r'	Propagation distance from real source to observer
R	Radius of acoustic hemisphere
t	Time of observation
U	Speed of source
x_0	Initial position of observer
$\vec{x}$	Position of observer
$\vec{x}_s$	Position of compact source
X	Speed of observer
$\vec{y}$	Position of acoustic source
θ	Elevation angle
τ	Time of emission
τ^*	Time of emission from compact source
ϕ	Phase
ψ	Azimuth angle
ω	Frequency of source
ω'	Apparent frequency at observer
$()_a$	Air-based
$()_g$	Ground-based

1. INTRODUCTION

It is well known that helicopter noise is comprised of both periodic and broadband noise sources with periodic sources dominating the noise signature in most cases. Thickness, loading, and impulsive noise sources, radiating from both the main and tail rotor, can all contribute to harmonic noise levels. When the source has impulsive events, like "Blade-Vortex Interaction" (BVI) noise and "High Speed Impulsive" (HSI) noise, the identification of the radiating noise sources is best done in the time domain, where both the phase and amplitude of the measurements are easily identified. For a helicopter in steady-state flight, the actual measurement and identification of these periodic emissions can be obtained by using several complementary measurement methods.

One method, that uses one or more flying microphones positioned at fixed distances from the helicopter, has been quite successful in quantifying impulsive noise radiation. The microphones are either mounted on the helicopter at fixed spatial positions,[1] or mounted on a lead aircraft that is flown in formation with the helicopter so that the distance between the microphones and the helicopter remain fixed.[2] Because the measurements are effectively fixed with respect to the sound source, the noise repeats at the fundamental frequency of the noise source. The relatively clean harmonic spectra and pressure time-histories of each sound source can often lead to high quality acoustic data that can be used for system identification and modeling of rotorcraft noise. Because the data are periodic, the data can be averaged in the time domain to further enhance the harmonic noise at the expense of more broadband noise sources.

Similarly, acoustic measurements that are made with

stationary microphones mounted in wind tunnels that have been treated with appropriate sound deadening material to reduce reflections from the surrounding walls, can also be used to measure impulsive noise. In this case, the helicopter (sound source) and the microphones are again fixed, while the wind tunnel moves the fluid (air) across the model and the measurement microphones. Once again, periodic signal averaging can be used to enhance the harmonic noise at the expense of broadband noise - helping separate harmonic noise from broadband noise and thus helping improve the understanding and identification of helicopter harmonic noise sources.

Perhaps a more common and direct way to measure helicopter noise is to use one or more microphones mounted to the ground and measure the radiated noise as the helicopter flies over the microphone or microphone array. In this case, the distances between the measurement microphones and the helicopter are continually changing, as are the directivity angles between the helicopter and the microphones. If periodic events are to be clearly identified and averaging techniques employed, the measured signal needs to be corrected for these effects. Correcting these acoustic signals by compensating for the changing position and motion of each helicopter sound source is the focus of this paper.

2. Background

De-Dopplerization is the term that is normally used to describe the process of trying to compensate for the position and motion of the helicopter in the signal analysis of ground based acoustic measurements. It is usually performed in the frequency domain, shifting the frequency of measured noise to compensate for the velocity of the aircraft with respect to the ground based microphones.[3] However, this approach assumes that the frequencies of the observed signal remain constant over the frequency analysis time window, when in reality the observed frequency content is continuously changing. This assumption often leads to a smearing of the frequency spectra of periodic noises, making it difficult to discriminate between rotor impulsive noise sources at higher frequencies.

Time domain de-Dopplerization approaches have also been attempted with some success.[4][5] In these approaches, it was assumed that all noise emanated from a single point on the helicopter. Using knowledge of the helicopter's velocity time-history, the acoustic signals were de-Dopplerized in an attempt to remove the effect of the helicopter's motion through the medium from the measured signals, creating a representation of the helicopter as a "stationary" source.

In this paper, a new time-domain approach to the problem is presented that expands upon and removes some of the limitations of the previous research. A new algorithm has been developed to de-Dopplerize the measured ground-based acoustic pressure time-history measurements to produce pressure time history signals equivalent to those that would be measured by "virtual inflight microphones" traveling with the helicopter through a fixed medium at fixed distances away from the helicopter. Corrections for the changing relative positions of the observers with respect to the harmonic noise sources are included - insuring that the resulting de-Dopplerized signal is periodic over the measurement interval. The new algorithm also employs signal averaging to further enhance the periodic signals emanating from the helicopter. Harmonic sources associated with the main rotor are separated from those of the tail rotor by averaging on the magnetic and simulated once per revolution signals, respectively. While advanced 2D spectral methods have been advocated for separation of main and tail rotor noise [6], they have only been demonstrated in conditions where the Doppler frequency shift remains constant over a limited range of directivity angles.

The new algorithm is then applied to measured ground acoustic data [7] for the Bell 206B3 helicopter. The main rotor and tail rotor harmonic noise due to several noise sources are effectively separated for two flight conditions with different noise radiation characteristics.

3. Theory

When a helicopter is in steady-state flight, it is creating harmonic noise that is associated with and necessary for powered flight. The resulting acoustic waves are propagated in the medium (air) and constitute the harmonic noise radiation of the helicopter. Motion of the helicopter has an effect on how the waves are deposited in the medium. Motion of the observer does not influence the sound field produced by the source, but does affect the acoustic pressure time-history as it is measured at the observer's location. The mechanism of the Doppler effect due to motion of both source and observer is described in this section, using the general equations for a sound source in motion.[8]

The general equation for the acoustic pressure observed at location $\vec{x}$ due to an acoustic source of strength q is given in Equation 1.

$$p'(\vec{x},t) = \int \frac{q(\vec{y},\tau)}{4\pi|\vec{x}-\vec{y}|} d^3\vec{y} \tag{1}$$

Where t is the time the acoustic pressure is observed at $\vec{x}$ and τ is the associated time at the source.

If the source is assumed to occupy a single point in space, $\vec{x}_s$, it may be expressed as follows:

$$q(\vec{y},\tau) = Q(\tau)\delta(\vec{y}-\vec{x}_s(\tau)) \tag{2}$$

Substituting into Equation 1:

$$p'(\vec{x},t) = \int_{-\infty}^{t} \int_V \frac{Q(\tau)\delta(\vec{y}-\vec{x}_s(\tau))}{4\pi|\vec{x}-\vec{y}|} d^3\vec{y}d\tau \tag{3}$$

By evaluating the point source at the single time of emission associated with the time of observation, the following expression is obtained using the retarded time equation:

$$p'(\vec{x},t) = \int_{-\infty}^{t} \int_V \frac{Q(\tau)\delta(\vec{y}-\vec{x}_s(\tau))}{4\pi|\vec{x}-\vec{y}|} \delta(t-\tau-\frac{|\vec{x}-\vec{y}|}{a_0}) d^3\vec{y}d\tau \tag{4}$$

Resolving the integral in space over the compact source:

$$p'(\vec{x},t) = \int_{-\infty}^{\infty} \frac{Q(\tau)\delta(t-\tau-\frac{|\vec{x}-\vec{x}_s(\tau)|}{a_0})}{4\pi|\vec{x}-\vec{x}_s(\tau)|} d\tau \tag{5}$$

A useful property of δ-functions is given in Equation 6.

$$\int_{-\infty}^{\infty} f(\tau)\delta(g(\tau))d\tau = \left[\frac{f(\tau)}{|\frac{dg}{d\tau}|}\right]_{\tau=\tau^*} \tag{6}$$

τ^* is the root of $g(\tau)$ - in this case, the retarded time equation.

$$g(\tau^*) = t - \tau^* - \frac{|\vec{x} - \vec{x}_s|}{a_0} = 0 \tag{7}$$

Carrying out the differentiation of the denominator, the result is dependent on the Mach number of the source *with respect to the medium* along the radiation direction between the source and observer.

$$\left|\frac{dg}{d\tau}\right| = \left|-1 + \frac{x_i - x_{si}}{|\vec{x} - \vec{x}_s|}\frac{1}{a_0}\frac{dx_{si}}{d\tau}\right| = |1 - M_r| \tag{8}$$

Substituting Equations 6 and 8 into Equation 5 results in the equation for the acoustic pressure generated by a moving point source. The point source is amplified by the Doppler amplification factor $|1 - M_r|$.

$$p'(\vec{x}, t) = \frac{Q(\tau^*)}{4\pi|\vec{x} - \vec{x}_s(\tau^*)|}\frac{1}{|1 - M_r|} \tag{9}$$

For a source traveling along direction x_1 at a constant speed U, the correct emission time τ^* can be calculated directly from a quadratic equation from the geometry shown in Figure 1. Taking the subsonic root yields Equation 10.

$$\tau^* = t - \frac{M(x_1 - Ut)}{a_0(1 - M^2)} - \frac{\sqrt{(x_1 - Ut)^2 + (1 - M^2)(x_2^2 + x_3^2)}}{a_0(1 - M^2)} \tag{10}$$

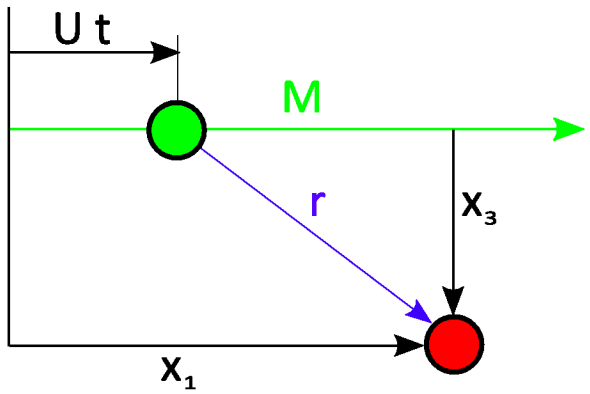

Fig. 1. **Equation 10 geometry, source (green) and observer (red).**

By substituting Equation 10 into Equation 9, the acoustic pressure generated by the moving source in the medium may be calculated for any point $\vec{x}$ at any time t. Motion of the observer is accounted for by defining the location of the observer within the medium, $\vec{x}$, as a function of observer time, t. It is this relation between source time, τ^*, and observer time, t, which causes the well known Doppler frequency shift by expanding or contracting the acoustic pressure time-history emitted by the source in time, as seen by the observer. (Figure 2)

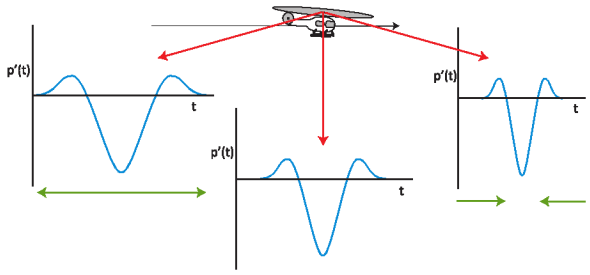

Fig. 2. **Time dilation of pressure time-history signal of a moving source as seen by a stationary observer.**

The classical frequency-domain expression for the Doppler frequency shift may be obtained from the retarded time expression given by Equation 10. For example, consider a simple harmonic source, as described by Equation 11. Let the source move at speed U in the same direction as the observer, moving at speed X as shown in Figure 3.

$$Q(\tau^*) = \sin(\omega\tau^*) \tag{11}$$

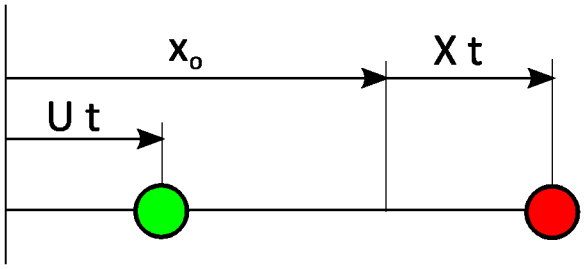

Fig. 3. **Simple 1-D geometry example, source (green) and observer (red).**

Using Equation 10 the apparent frequency seen by the observer can be readily determined. Applying the source and observer geometry shown in Figure 3 to Equation 11 yields,

$$\begin{aligned}\tau^* &= t - \frac{M(Xt + x_0 - Ut) - \sqrt{(Xt + x_0 - Ut)^2}}{a_0(1 - M^2)} \\ &= t - \frac{M_o t + x_0 - Mt}{(1 - M)} = \frac{1 - M_o}{1 - M}t + \frac{x_0}{a_0(1 - M)}\end{aligned} \tag{12}$$

Substituting Equation 12 into 11 yields the well known frequency-domain expression for the change in observed frequency due to the motions of the source and observer.

$$\begin{aligned}Q(t) &= \sin(\omega\frac{1 - M_o}{1 - M}t + \omega\frac{x_0}{a_0(1 - M)}) \\ &= \sin(\omega' t + \Delta\phi) \\ \text{where } \omega' &= \frac{1 - M_o}{1 - M}\omega\end{aligned} \tag{13}$$

However, when the direction of propagation does not lie along the direction of motion of both the source and the observer, the change in apparent frequency is no longer constant in time. Instead, the Mach numbers of the source and observer as measured along the direction of propagation vary over time yielding a time-varying change in the apparent frequency. This effect is fully accounted for in Equation 10, which is valid for any motion of the observer relative to the moving source.

4. Sample Calcuation

The case of a moving point source with strength varying harmonically, as described in Equation 11, is considered

for three observer geometries. The source motion is similar to that of a helicopter during a level flight flyover, and is described in Table I. The observer geometry is described in Table II. The first observer geometry is that of a typical ground-based microphone, stationary with the medium. The second is an air-based observer which travels a fixed distance away from the source, but sweeps along the same elevation angles covered by the ground-based observer during the flyover. The third observer also travels with the source, but maintains a constant elevation angle as well a distance, analogous to a stationary wind tunnel or inflight measurement. The ground- and air-based observer geometries are shown in Figure 4 and are evaluated using Equation 10. The wind tunnel geometry is similar to the air-based geometry, except that observer travels with the source at a fixed angle such that the relative velocity between the observer and source is exactly zero. As such, the signals observed by the air-based and wind tunnel observers are nearly identical.

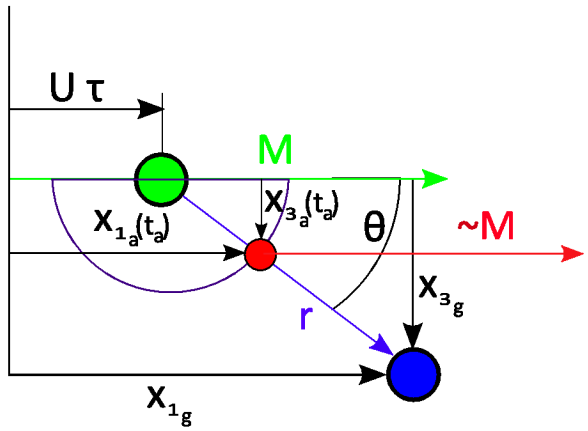

Fig. 4. **Ground- (blue) and air- (red) based observer geometries, as evaluated by Equation 10.**

TABLE I
Sample calculation parameters.

U	170	ft/s
a_0	1100	ft/s
R	30	ft
ω	15 & 150	Hz
f_s	20	kHz

TABLE II
Observer locations.

	Ground	Air-Based	Wind Tunnel
x_1	1000 ft	$Ut + R\cos(\theta_g)$	$Ut + R\cos(\pi/4)$
x_2	0	0	0
x_3	492 ft	$-R\sin(\theta_g)$	$R\sin(\pi/4)$

where θ_g is the elevation angle of the ground based observer, i.e. $\tan(\theta_g) = x_{3g}/x_{1g}$

Figure 5 shows the resulting pressure time-history for the 15 Hz source at all three observers for the first 0.2 seconds of the simulated flyover. Amplitudes of all three signals are approximately equal, however due to the continuously decreasing time delay between the moving source and the stationary ground observer, the signal observed on the ground is compressed in the time domain.

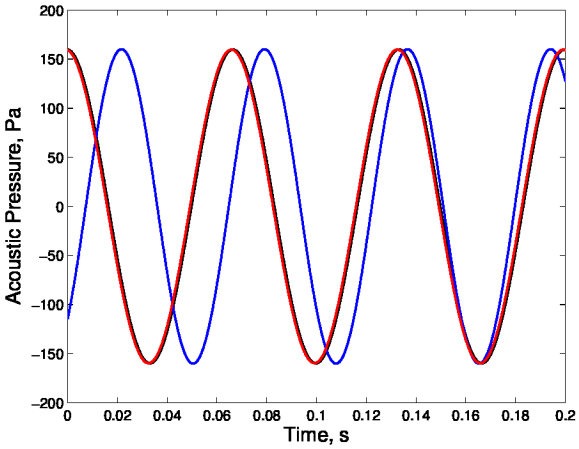

Fig. 5. **Pressure time-history of 15Hz signal observed by: ground (blue), inflight (red), wind tunnel (black).**

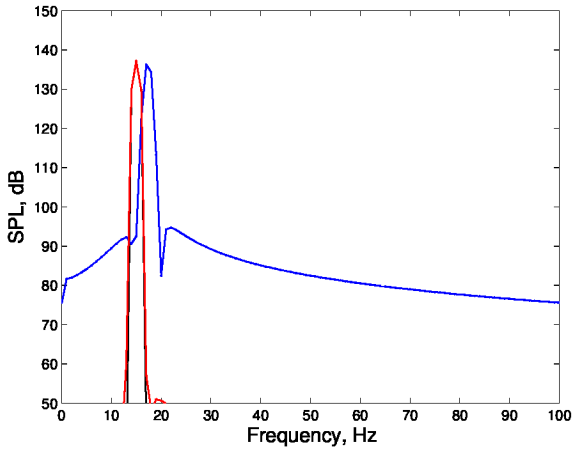

Fig. 6. **Frequency spectra of first second of 15Hz signal observed by: ground (blue), inflight (red), wind tunnel (black).**

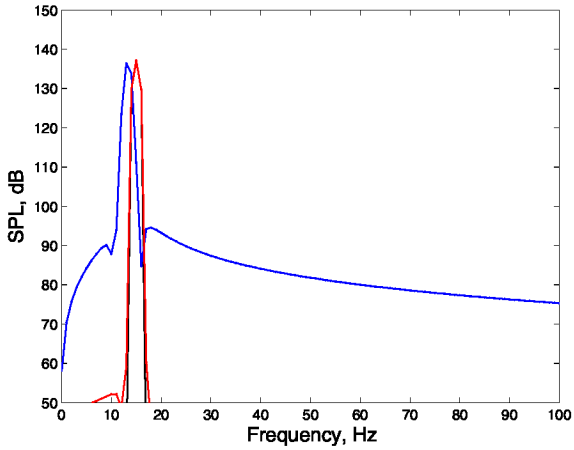

Fig. 7. **Frequency spectra of last second of 15Hz signal observed by: ground (blue), inflight (red), wind tunnel (black).**

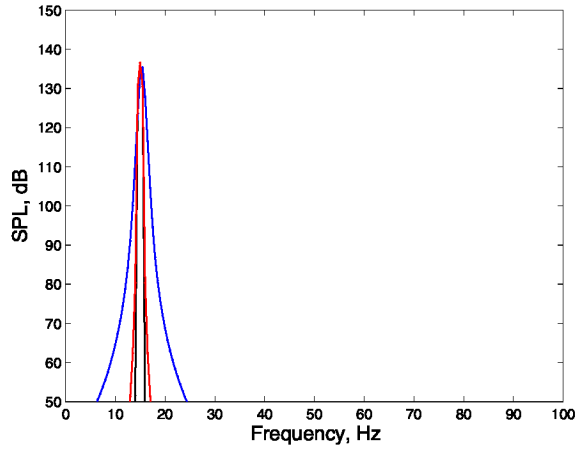

Fig. 8. **Frequency spectra of middle second of 15Hz signal observed by: ground (blue), inflight (red), wind tunnel (black).**

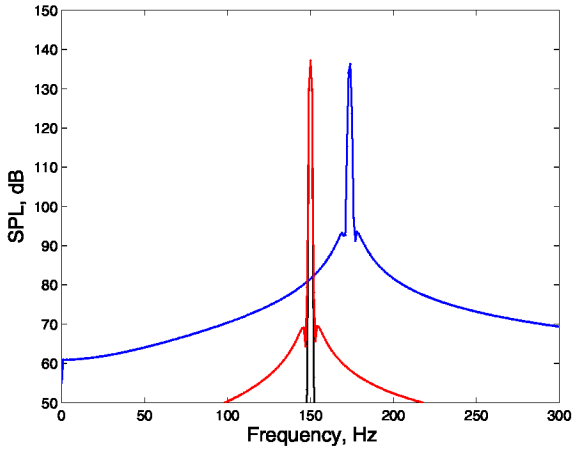

Fig. 9. **Frequency spectra of first second of 150Hz signal observed by: ground (blue), inflight (red), wind tunnel (black).**

Figures 6, 7, and 8 show the frequency spectra of the signals as observed during the first, last, and middle second of the flyover, respectively. During the first second of the flyover, the source is approaching the ground-based observer. During the middle second of the flyover, the source passes overhead the ground-based observer. During the last second the source travels away from the ground-based observer. The frequency spectra are calculated using a Hann window over one second of data, in order to reduce spectral leakage. The air-based signal appears as a steady 15Hz tone in all three spectra, as does the wind tunnel signal. However, the peak value of the ground-based signal is shifted in frequency, increasing as the source moves towards the observer and decreasing as the source moves away. More importantly, the frequency spectra for the ground-based signal is “smeared” across a broader range of frequencies, because the time-delay between source and observer varies throughout the one second frequency spectra window. The “smearing” is most severe when the source passes directly overhead, since the rate of change of the directivity angle (i.e. slew rate) is highest. “Smearing” of the inflight spectra is minimal due to the slight motion between the source and observer. As expected, no “smearing” is observed for the stationary wind tunnel observer, producing a frequency spectra nearly identical to that seen by the air-based observer.

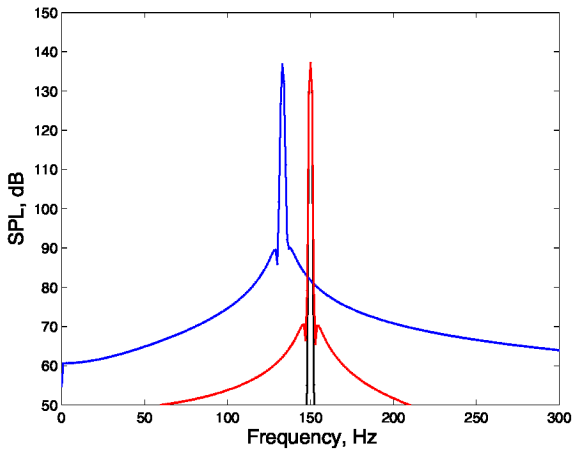

Fig. 10. **Frequency spectra of last second of 150Hz signal observed by: ground (blue), inflight (red), wind tunnel (black).**

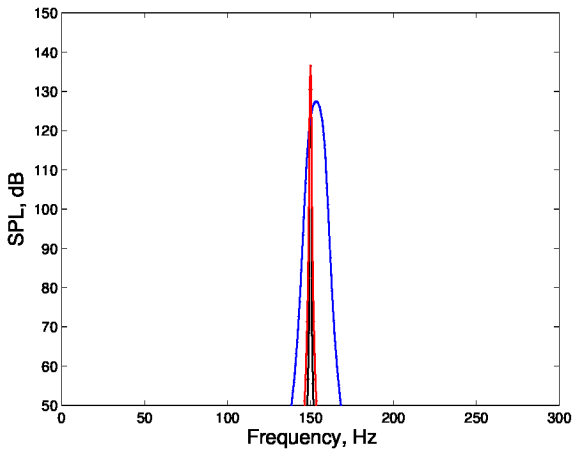

Fig. 11. **Frequency spectra of middle second of 150Hz signal observed by: ground (blue), inflight (red), wind tunnel (black).**

Figures 9, 10, and 11 show the same frequency spectra for the 150 Hz source. A greater shift in frequency content is observed.

The case of a square pulse source is also analyzed. The pressure time-history observed for a square pulse source with a 10% duty cycle activated at 15 Hz is shown in Figure

12. Again, the observed signal is compressed or expanded in time due to the change in retarded time, but the pulse shape is not distorted.

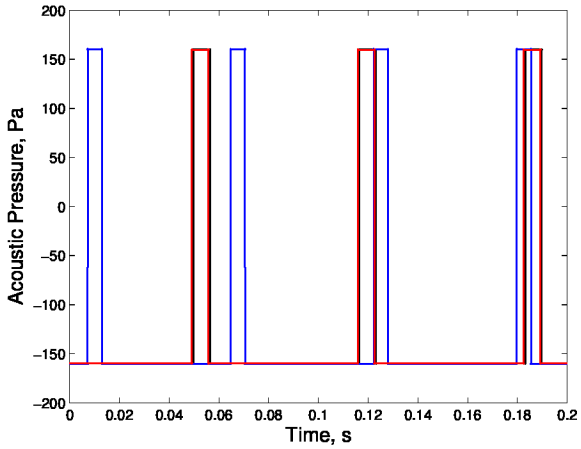

Fig. 12. **Pressure time-history of square pulse signal observed by: ground (blue), inflight (red), wind tunnel (black).**

Figures 13, 14, and 15 show the first, last, and middle second frequency spectra for the square pulse source. The effect of frequency "smearing" masks the clear 15 Hz harmonic peaks produced by the square pulse for the ground-based observer, especially for the middle second where the source is flying directly over the observer and the geometry between the source and observer changes most rapidly. The tonal content of the source remains distinct for the inflight observer throughout the simulated flyover and is nearly identical to that observed in the wind tunnel case.

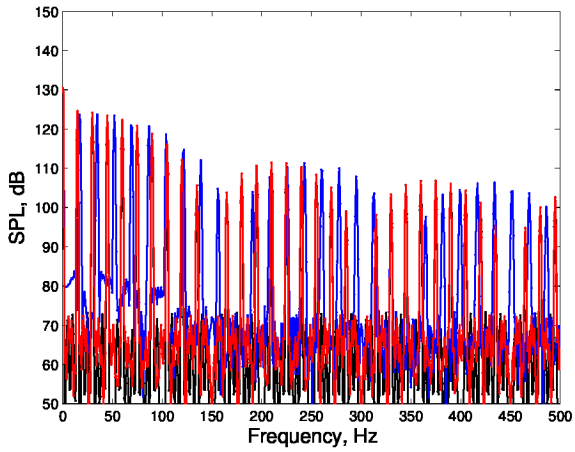

Fig. 13. **Frequency spectra of first second of square pulse signal observed by: ground (blue), inflight (red), wind tunnel (black).**

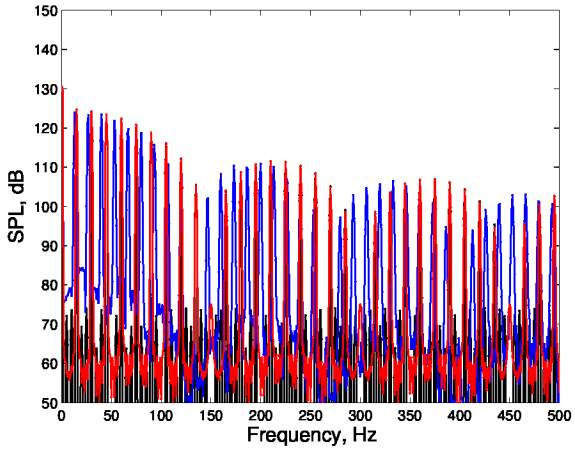

Fig. 14. **Frequency spectra of last second of square pulse signal observed by: ground (blue), inflight (red), wind tunnel (black).**

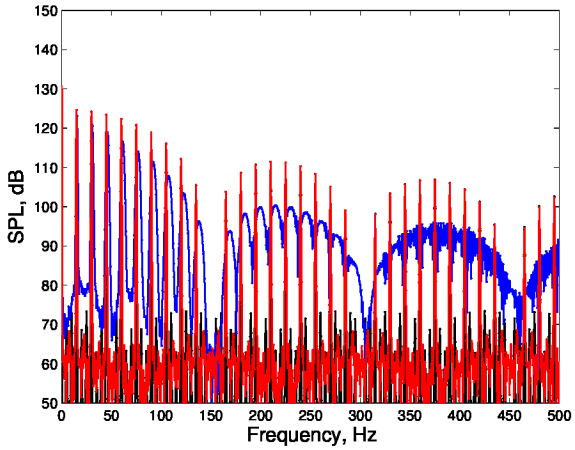

Fig. 15. **Frequency spectra of middle second of square pulse signal observed by: ground (blue), inflight (red), wind tunnel (black).**

The "smearing" of the frequency of the source due to the Doppler effect is clearly evident in all of the ground-based measurements. All observers, however, are subject to the same Doppler amplification, since this is determined by the Mach number of the source with respect to the medium. Regardless, for typical helicopter flight speeds, ($M < 0.2$) the effect of Doppler amplification due to the velocity of the helicopter through the medium is negligible. For example, for $M = 0.2$ (~130 kts at sea level) the maximum possible Doppler amplification due to overall helicopter motion is only 0.35 dB.

5. Application

Following a time-domain extension of the Rotorcraft Noise Model (RNM) methodology [9] [10], the helicopter is modeled as a compact source. The magnitude and directivity of the noise radiated by this source is described on a hemispherical surface which moves with the helicopter at a fixed radius away from the source. The pressure time-history observed at a "virtual inflight microphone" moving along the surface of this hemisphere may be generated

from the ground-based microphone pressure time-history signal by evaluating the retarded time, as shown in Equation 7. For a compact source, this "virtual microphone" is equivalent to the air-based observer described in the previous section. At each time-history sample of the observed signal the time of emission from the compact source is calculated as well as the theoretical time of observation at the "virtual microphone" at a position along the assumed straight-line propagation path between the source at the time of emission and the ground-based observer at the time of reception. (Figure 16) In addition to the time shift between the ground-based observer and the "virtual" observer, Equation 9 shows that there is also a change in amplitude due to spherical spreading - however, there will be no change in amplitude due to Doppler amplification. The Doppler amplification of the source is the same for both observers as neither the Mach number of the source with respect to the medium nor the direction of observation varies.

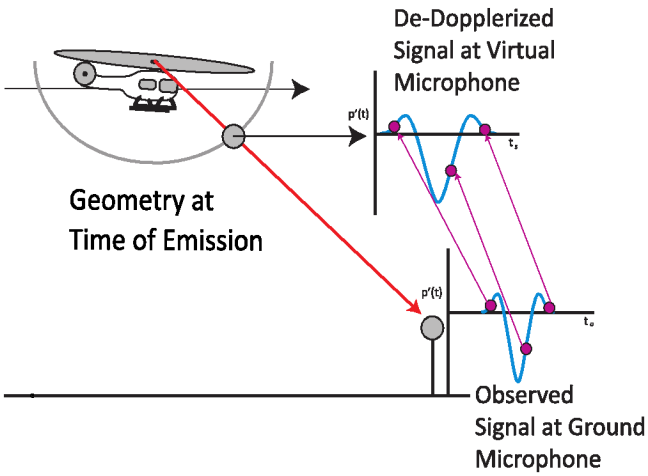

Fig. 16. **Time-history de-Dopplerization process.**

The process of de-Dopplerizating the pressure time-history data is as follows:

1) The helicopter pressure time-history and position tracking data are discretized in time at fixed sampling rates.
2) The position tracking data is discretized at a lower sampling rate than the pressure time-history data. A continuous piecewise-defined spline is fit to the tracking data in order to provide tracking data at arbitrary time steps.
3) For each acoustic sample, the correct time of emission, time of observation at the spherical surface, and position of the helicopter along the track are calculated. For a real trajectory, this solution is iterative but convergence is quick. The iterative solution may be initialized by assuming straight-line motion of the helicopter between known position tracking points, for which the retarded time is known exactly from Equation 10.
4) Using the propagation distance calculated at each time-history sample, the change in amplitude due to spherical spreading may be calculated and applied for each individual pressure time-history sample. The de-Dopplerized signal observed by the "virtual inflight microphone" may now be obtained.
5) The time steps between samples of the transformed signal are non-uniform. In order to calculate frequency spectra using standard techniques the signal must be resampled to a fixed time-step. This process may introduce aliasing at a lower frequency than for the untransformed signal. An increase of the initial sampling rate by 30% has been recommended. [11] However, the Non-Uniform Time Discrete Fourier Transform [12] [13] can be used to calculate uniform frequency spectra without affecting the Nyquist frequency, as the average sampling frequency of the non-uniformly spaced signal does not change significantly.

Having transformed the signal from the ground-based observer to the inflight observer, standard periodic averaging techniques may be applied to the time-history data in order to separate the main rotor periodic and tail rotor periodic noise sources. Since the angular velocity of the rotor may vary by as much as $\pm 3\%$ over the course of the data collection run, a magnetic once per revolution sensor is used to divide the inflight pressure time-history signal into main rotor periods. At the directivity angles corresponding to the ground microphone measurements made at known positions of the helicopter, about one second worth of rotor revolutions of signals are collected. These signals are then scaled in time to match the average period of the main rotor, and then ensemble averaged. For instance, for a rotor with a 6.5 Hz rotational frequency, seven rotor periods will be averaged together, with three preceding the period containing the exact time of emission associated with current directivity angle and three following. During actual inflight noise measurement more rotor revolutions are used to periodically average the signal;[1] however, in these cases the directivity angle of the observer and the source remains fixed. This is not the case when constructing a "virtual inflight microphone" from ground-based measurements. Since the "virtual inflight microphone" must change directivity angle with the ground-based observer used to construct it, the signal is not truly stationary. One second of data was found to adequately suppress the unwanted non-periodic signals while averaging over a short enough period of time so that the observed pressure time-history signal does not change significantly from one period to the next. Tail rotor periodic data is processed in a similar fashion as the main rotor data, except that the main rotor once per revolution sensor is used to synthesize the tail rotor periods from a known fixed gear ratio between the main rotor and tail rotor. [14]

Typically, acoustic hemispheres are generated assuming all noise produced by the helicopter may be represented by a compact source located at the main rotor hub. In reality, the noise is generated by a distribution of sources across the rotor blades which vary azimuthally in strength. The assumption of a hub-centered compact source introduces an error in the phase of the acoustic pressure originating from sources away from the hub during the evaluation of the retarded time equation. For lower frequency sources, such as steady loading and thickness noise, the error in phase is relatively small. However, for impulsive noise sources like those associated with BVI, even a small change in phase can disrupt the averaging process. The error in phase is dependent on the geometry between the observer, the assumed source location, and the real source. A simplified

2D representation of the problem is shown in Figure 17.

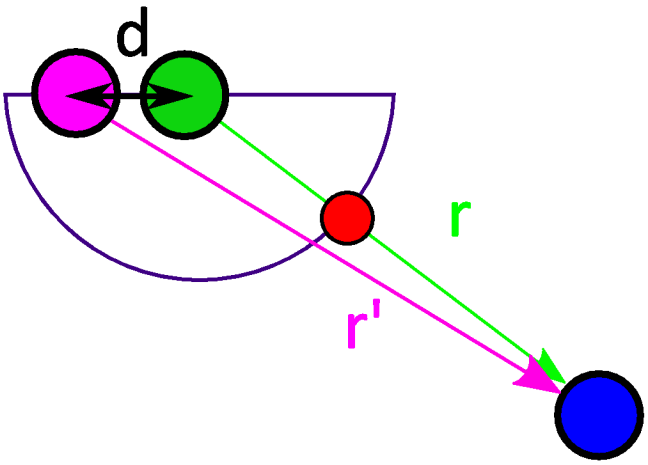

Fig. 17. **2-D example of phase difference due to error in assumed source location. Assumed source (green), "real" source (purple), ground observer (blue), virtual observer (red).**

When the observer is in the plane containing the assumed source location and the real source, the error in retarded time calculation will be the distance d divided by the speed of sound a_0. When the observer is directly underneath the two sources, the error in the retarded time calculation will be zero, as the path lengths r and r' will be equal. (Fig. 18) If the observer is much farther from the sources than the distance d, the error in retarded time may be approximated using Equation 14. More significantly for the averaging process, the rate of change of the error in the retarded time calculation is highest out of the plane between the assumed source and the real source, as shown in Figure 19, calculated from Equation 10.

$$\Delta t = \frac{d}{a_0}\cos(\theta) \tag{14}$$

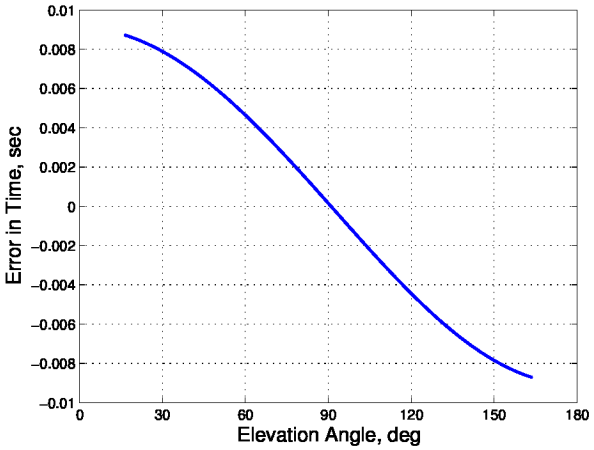

Fig. 18. **Error in retarded time calculation due to 10' displacement of real source during a level flyover at 492' altitude.**

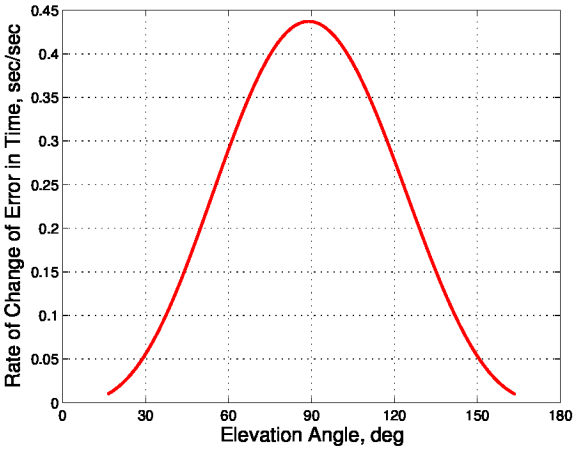

Fig. 19. **Rate of change of error in retarded time calculation due to 10' displacement of real source a level flyover at 492' altitude.**

For the case of a real helicopter, all sources are on or near the rotor blades. Several different BVIs may occur at once, originating from different locations on the rotor disk. At the elevation angles underneath the rotor plane, the phase of the BVI pulse will shift quickly between each rotor period, eliminating the BVI pulse from the averaged signal. The error in the assumed source location is not as important in the plane of the rotor because the rate of change of phase due to error in the retarded time calculation is small. Therefore, the BVIs which radiate the most noise below the helicopter are the most sensitive to error in source location.

The hemisphere could be constructed about a different assumed source location on the rotor, more representative of BVI. However, different types of BVI occur during different flight conditions, occurring at different areas on the rotor disk. For example, a parallel BVI may occur on a 2-bladed rotor at about 45° azimuth, and occurs across much of the blade simultaneously. Oblique BVIs occur across a range of azimuths, and sweep across the blade over time. Since it is difficult to predict which BVI will be dominant for a particular flight condition *a priori* it is useful to correct for the error in the phase of BVI pulses individually at each directivity angle on the surface of the acoustic hemisphere. The most prominent BVI pulses in the signals are synchronized between revolutions by adjusting the phase of each time segment used in the periodic average through a minimization of the norm of the difference between the pressure time history of the central signal in the average and all other signals composing the periodic average.

6. Results

The methods of de-Dopplerization and rotor noise source separation developed in this paper are applied to ground-based measurements of the Bell 206B3 helicopter collected by the University of Maryland, Bell Helicopter, and NASA in 2007. A seven-position ground microphone array composed of both ground-board and 1.2m FAA noise certification microphones was employed to capture acoustic data across a wide range of directivity angles for the Bell 206B3 during numerous steady-flight conditions. Details of the flight test setup are available from Reference [10]. The methods

developed in this paper are applied to two flight conditions from this dataset: one where the magnitude and directivity of externally radiated noise is dominated by the tail rotor and the other where they are dominated by the main rotor.

The first flight condition considered is level flight at 60 kts, where the external acoustic radiation is known to be dominated by the tail rotor in the BVISPL frequency range. [14][7][10] In this paper, BVISPL is defined as the unweighted sound pressure level of all noise between the 5^{th} and 60^{th} harmonics of the blade passage frequency. The acoustic hemispheres presented in this paper are displayed using a Lambert projection, in order to allow an undistorted picture of the external noise radiation pattern. The process of projecting the hemispherical surface as a 2D image using the Lambert projection is shown in Figure 20. The center of the plot, marked with an elevation angle of -90° represents the underside of the hemisphere. The edges with a 0° elevation represent noise radiated in the horizon plane. Azimuth angles start at 0° behind the helicopter, and progress counter-clockwise with the direction of the Bell 206 rotor so that the right hand side of the plot represents the advancing side of the hemisphere. The markers on the plot indicate the directivity angles at which BVISPL values have been evaluated from the virtual microphone pressure time-histories - these values are then interpolated to generate BVISPL contours along the surface of the hemisphere. Figure 21 shows the acoustic hemisphere of BVISPL generated from the unaveraged pressure time-history signals. Tail rotor thickness noise radiates ahead of the helicopter, setting the directivity pattern.

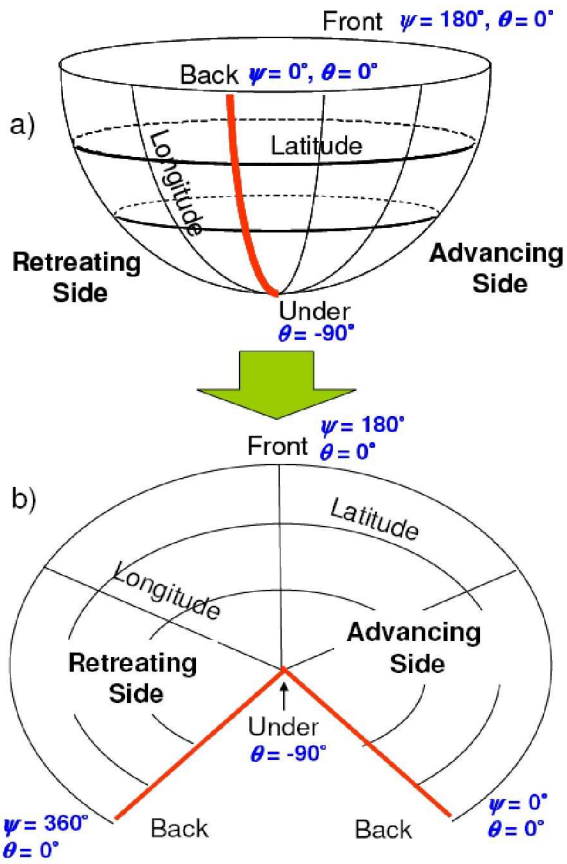

Fig. 20. **Lambert conformal conic projection of an acoustic radiation hemisphere.**

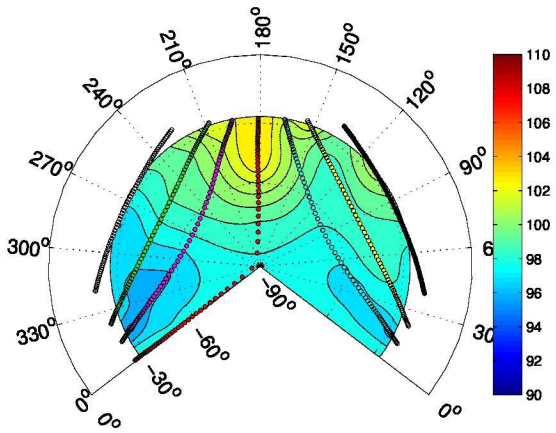

Fig. 21. **Unaveraged 60 kts level flight BVISPL (dB) hemisphere contours.**

Figure 22 shows the hemisphere produced by averaging the processed "virtual inflight" pressure-time histories on the synthesized tail rotor once per revolution signal. As expected, the resulting magnitude and directivity of the tail rotor averaged hemisphere closely match those of the unaveraged hemisphere, since the BVISPL in this flight condition is dominated by the tail rotor.

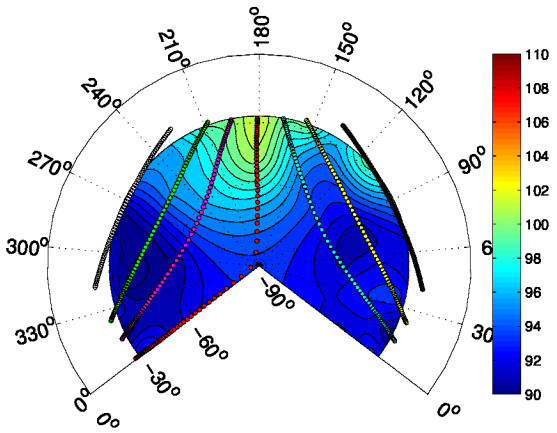

Fig. 22. **Tail rotor averaged 60 kts level flight BVISPL (dB) hemisphere contours.**

The main-rotor averaged hemisphere for the level flight condition is shown in Figure 23. The magnitude of the main rotor periodic noise is less than that of the tail rotor. The noise radiates ahead of the helicopter, but at a lower elevation angle than that of the tail rotor thickness noise.

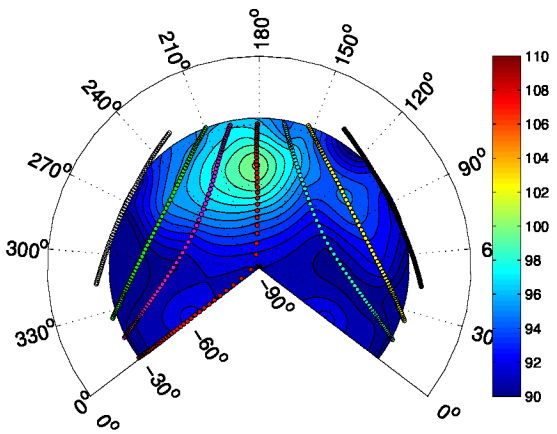

Fig. 23. **Main rotor averaged 60 kts level flight BVISPL (dB) hemisphere contours.**

The BVISPL noise radiation characteristics of the Bell 206 are known be dominated by main rotor BVI in the 60kts, 6° descent angle condition. [14][7][10] The BVISPL levels of the unaveraged hemisphere are shown in Figure 24. Overall BVISPL are higher in this flight condition. In addition, the directivity pattern is shifted towards the advancing side.

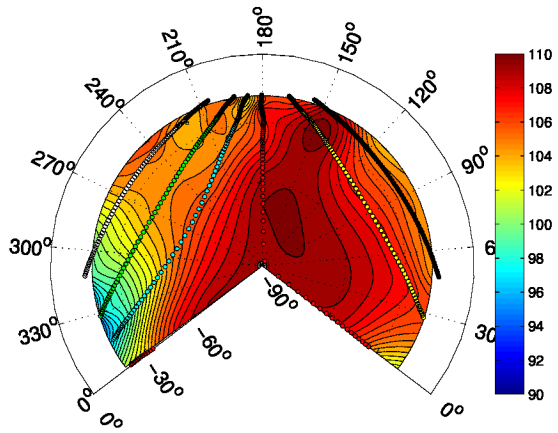

Fig. 24. **Unaveraged 60 kts descending BVISPL (dB) hemisphere contours.**

Figure 25 shows the directivity pattern of the tail rotor averaged hemisphere. The directivity pattern is very similar to that observed in the level flight case - this is to be expected as tail rotor thickness noise should not be affected by descent angle.

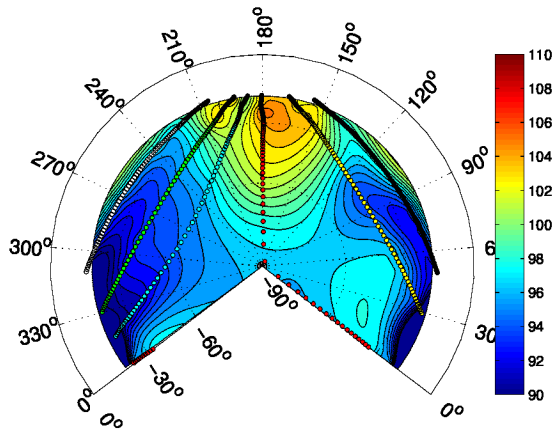

Fig. 25. **Tail rotor averaged 60 kts descending BVISPL (dB) hemisphere contours.**

Thus far, the BVISPL contours of the phase-corrected and uncorrected periodically averaged hemispheres have been indistinguishable, due to the lack of periodic BVI pulses in the measured pressure time-history signals. The correction becomes necessary when evaluating main rotor averaged hemispheres during flight conditions with significant BVI noise. The hub-centered hemisphere resulting from the main rotor averaged signals without phase correction for BVI pulses is plotted in Figure 26. The peak BVISPL "hotspot" near -30° elevation angle is accurately captured by the averaging scheme. As expected, BVISPL levels are significantly reduced in the directivity angles near the bottom of the hemisphere. A closer examination of the time-history signals recorded by the "virtual inflight microphones" shows the sensitivity of BVI noise to the phase error caused by evaluating the retarded time equation for a hub-based source.

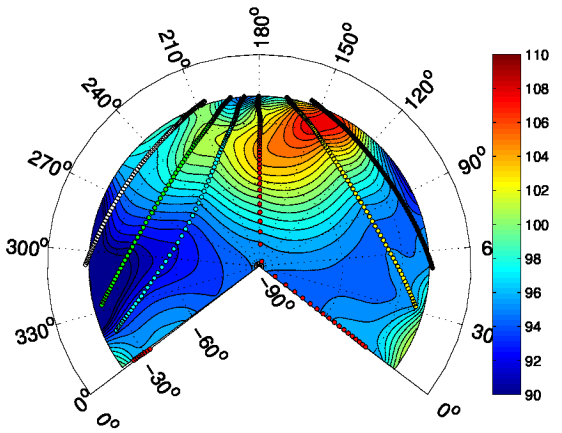

Fig. 26. **Main rotor averaged 60 kts descending BVISPL (dB) hemisphere contours, without phase correction.**

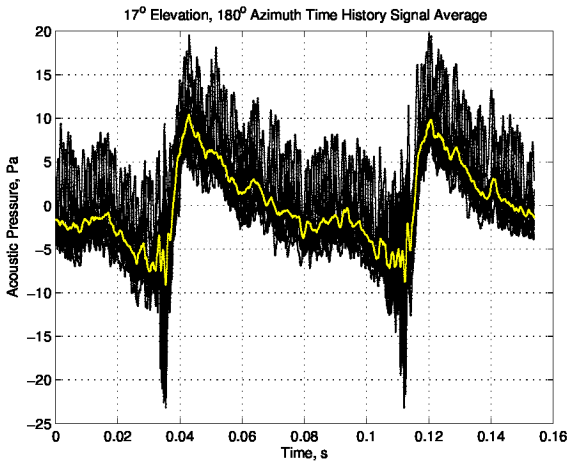

Fig. 27. **Near inplane time-history signals: averaged (yellow), unaveraged (black).**

Figure 27 shows the averaged pressure time history signal superimposed over the fourteen unaveraged main rotor period signals measured directly ahead of the helicopter at the nearest measured point to the plane of the rotor, at 17° below the horizon. The main rotor does not radiate much BVI noise in this direction, however the averaging technique captures the main rotor lower harmonic noise very well.

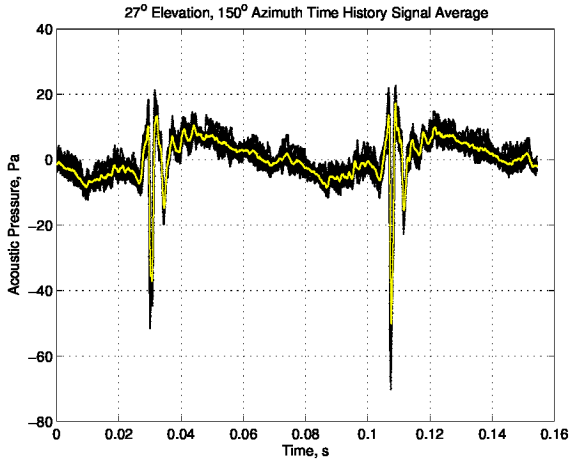

Fig. 28. **Peak BVI direction time-history signals: averaged (yellow), unaveraged (black).**

Figure 28 shows the averaged and unaveraged signals captured at the BVISPL hotspot on the sphere. The strong BVI pulse is well captured by the averaging method at this location.

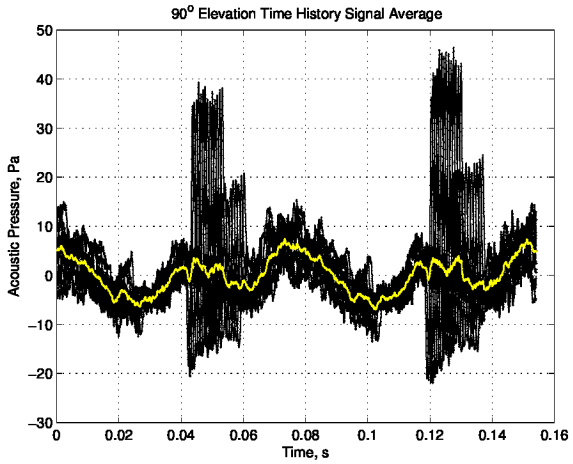

Fig. 29. **Uncorrected out of plane time-history signals: averaged (yellow), unaveraged (black).**

Figure 29 shows the pressure time-history measured on the underside of the hub-centered hemisphere. In this case, where the phase error of the BVI pulse is changing rapidly over time, the BVI pulse is not retained in the averaged pressure time-history signal.

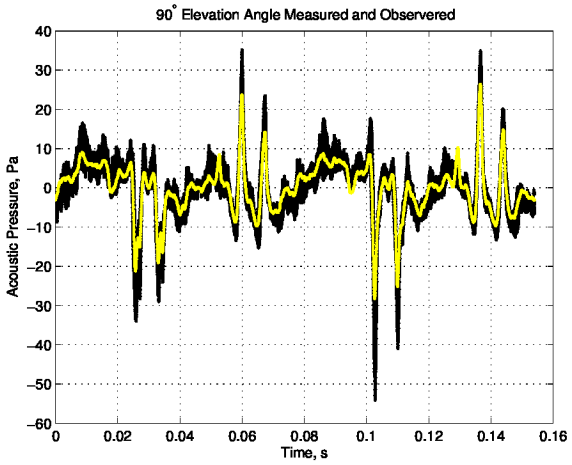

Fig. 30. **BVI phase corrected out of plane time-history signals: averaged (yellow), unaveraged (black).**

Figure 30 shows the pressure time-history signals at the -90° elevation angle locations when the phase correction is applied. The phase correction scheme accurately synchronizes the BVI pulses without substantially affecting the lower frequency main rotor steady harmonic noise. The resulting BVISPL hemisphere is shown in Figure 31 - the BVISPL contour retains the magnitude and directivity of the BVI noise observed in the unaveraged case.

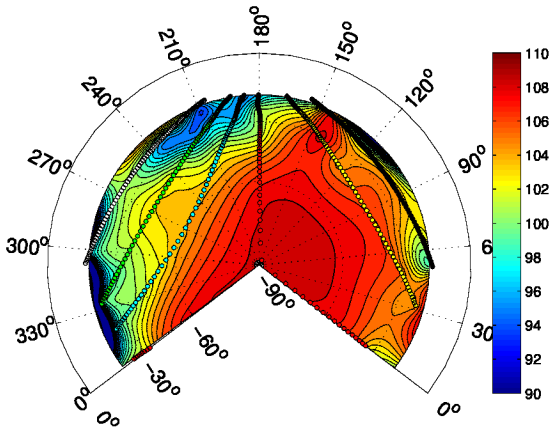

Fig. 31. **Main rotor averaged 60 kts descending BVISPL (dB) hemisphere contours, with BVI phase correction.**

7. Conclusions

A new method of transforming ground-based pressure time-history signals to those that would be observed by a "virtual inflight microphone" has been developed and successfully demonstrated. This technique eliminates the frequency "smearing" introduced by the Doppler effect into frequency spectra calculated from ground-based data and allows ground-based pressure time-history signals to be analyzed like those collected by wind tunnel testing or inflight observers but at greatly reduced cost. This new method is unique in that the effects of impulsive noise sources originating from different points on the rotor disk are accounted for using a phase-correction scheme applied to each rotor period. Using this new method, the pressure time-history signals may be periodically averaged in order to evaluate rotor harmonic noise sources, including impulsive noise such as BVI. This technique can be applied to noise measurements made at all points during the flyover, allowing accurate representations of the periodic pressure time-history signals associated with each rotor to be generated across a wide range of directivity angles. The methods developed in this paper were applied to ground-based microphone measurements of the Bell B206B3 helicopter in order to generate separate acoustic radiation hemispheres for the main rotor and the tail rotor. Hemispheres were generated for two different flight conditions, one where tail rotor noise dominates and one where main rotor BVI noise is dominant. This method provides a new tool enabling the identification and understanding of helicopter harmonic noise sources.

References

[1] B. W. Sim, T. Beasman, F. H. Schmitz, and G. Gopalan, "In-Flight Blade-Vortex Interaction (BVI) Noise Measurements Using a Boom-Mounted Microphone Array," in *the American Helicopter 60th Annual Forum Proceedings*. American Helicopter Society, June 2004.

[2] F. H. Schmitz and D. Boxwell, "In-Flight Far-Field Measurement of Helicopter Impuslive Noise," *Journal of the American Helicopter Society*, vol. 21, no. 4, October 1976.

[3] G. Howell, A. Bradley, M. McCormick, and J. Brown, "De-Dopplerization and Acoustic Imaging of Aircraft Fly-Over Noise Measurements," *Journal of Sound and Vibration*, vol. 105, no. 1, 1986.

[4] J. J. Kelly and M. R. Wilson, "De-Dopplerization of Aircraft Acoustic Signals," *Journal of Aircraft*, vol. 32, no. 5, pp. 1012–1017, September-October 1995.

[5] A. S. Babkin, "Signal Restoration of Non-Stationary Acoustic Signals in the Time Domain," NASA, CR-181627, April 1988.

[6] O. L. Santa Maria, "2-D Fourier Analysis of Helicopter Flyover Noise," Master's thesis, Pennsylvania State University, December 1998.

[7] F. H. Schmitz, E. Greenwood, R. D. Sickenberger, G. Gopalan, B. W. Sim, D. A. Conner, E. Moralez, and W. A. Decker, "Measurement and Characterization of Helicopter Noise in Steady-State and Maneuvering Flight," in *the American Helicopter 63rd Annual Forum Proceedings*, 2007.

[8] P. M. Morse and K. U. Ingard, *Theoretical Acoustics*. McGraw-Hill, 1986.

[9] D. A. Conner and J. A. Page, "A Tool for Low Noise Procedures Design an Community Noise Impact Assessment: The Rotorcraft Noise Model (RNM)," in *the Heli Japan 2002 Proceedings*, 2002.

[10] E. Greenwood, "A Physics-Based Approach to Characterizing Helicopter External Noise Radiation from Ground-Based Noise Measurements," Master's thesis, University of Maryland, November 2008.

[11] H. Kook, G. Moebs, P. Davies, and J. Bolton, "An Efficient Procedure for Visualizing the Sound Field Radiated by Vehicles During Standarized Passby Tests," *Journal of Sound and Vibration*, vol. 233, no. 1, pp. 137–156, May 2000.

[12] D. M. Bland, T. I. Laakso, and A. Tarczynski, "Analysis of Algorithms for Nonuniform-Time Discrete Fourier Transform," IEEE, 7803-3073, 1996.

[13] V. Liepin'sh, "A Spectral Estimation Method of Nonuniformly Sampled Band-Limited Signals," *Automatic Control and Computer Sciences*, vol. 28, no. 2, pp. 66–73, 1994.

[14] D. C. Sargent, "In-Flight Array Measurements of Tail Rotor Harmonic Noise," Master's thesis, University of Maryland, 2008.